Estimation of Area-Averaged Rainfall over Tropical Oceans from Microwave Radiometry: A Single Channel Approach

KYUNG-SUP SHIN,* PHIL E. RIBA, AND GERALD R. NORTH

Climate System Research Program, Department of Meteorology, Texas A&M University, College Station, Texas

(Manuscript received 17 March 1989, in final form 23 April 1990)

ABSTRACT

This paper presents a new simple retrieval algorithm for estimating area–time averaged rain rates over tropical oceans by using single channel microwave measurements from satellites. The algorithm was tested by using the Nimbus-5 Electrically Scanning Microwave Radiometer (ESMR-5) and a simple microwave radiative transfer model to retrieve seasonal 5° × 5° area averaged rainrate over the tropical Atlantic and Pacific from December 1973 to November 1974.

The brightness temperatures were collected and analyzed into histograms for each season and in each grid box from December 1973 to November 1974. The histograms suggest a normal distribution of background noise plus a skewed rain distribution at the higher brightness temperatures. By using a statistical estimation procedure based upon normally distributed background noise, the rain distribution was separated from the raw histogram. The radiative transfer model was applied to the rain-only distribution to retrieve area-time averaged rainrates throughout the tropics. An adjustment for the beam filling error was incorporated in the procedure.

Despite limitations of single channel information, the retrieved seasonal rain rates agree well in the open ocean with expectations based upon previous estimates of tropical rainfall over the oceans. We suggest that the beam filling correction factor is the most important, but least understood parameter in the retrieval process.

1. Introduction

The Tropical Rainfall Measuring Mission (TRMM; Simpson et al. 1988) has been proposed for precipitation measurements from a low altitude orbiting satellite. The main goal of the mission is to produce a monthly mean time series of average rainrates over 5° by 5° boxes over the tropical oceans. The combination of passive and active microwave sensors and visible/infrared radiometers will overcome some previous limitations on rainrate measurements from space. The proposed orbit of TRMM, low altitude (350 km) and low inclination (35°), has several distinct advantages. By confining the observations to only approximately half of the earth's surface area, the sampling errors will be reduced (North 1987). The lower altitude will lead to smaller footprints and presumably reduce beam filling errors (Chiu et al. 1990; Short and North 1990); the lower altitude also leads to lower requirements on antenna size and radar power. The lower inclination orbit also leads to a precession through the local hours of the day and in the course of a few weeks all local times are sampled uniformly.

The objective of this study is to propose and test a simple algorithm to retrieve area–time averaged rainrates over global scales in anticipation of TRMM. We also anticipate the analysis of existing single channel microwave data sets in order to improve our understanding of the global hydrological system between now and the time of launch of new missions. Our approach makes use of only a single channel microwave observation and is limited to tropical oceanic rainfall. It is well known that rainfall retrieval from single channel information is limited by variable surface emissivity for different surface characteristics, atmospheric water vapor, and nonraining cloud liquid water content. An approach utilizing multichannel information is desirable in principle, and has been studied by many previous investigators (Huang and Liou 1983, Wu and Weinman 1984, Kummerow 1987, Smith and Mugnai 1988, and many others). Smith and Kidder (1978) also attempted to use multispectral information on rainfall retrieval.

Retrieval of area–time averaged rainfall over oceans from single channel information is immensely helped by the relatively uniform ocean background. Some biases due to changing atmospheric conditions can be adjusted satistically if their characteristics can be identified for a long time and over wide areas. Similar stud-

* Present Affiliation: Korea Meteorological Service, Seoul, Korea.

Corresponding author address: Professor Gerald R. North, Department of Meteorology, Texas A&M University, College Station, TX 77843.

ies have been attempted by Kidder and Vonder Haar (1977) for depicting rainfall frequencies over oceans, and by Rao et al. (1976), who produced a Global Oceanic Rainfall Atlas using the Nimbus-5 Electrically Scanning Microwave Radiometer (ESMR-5). The same dataset used by Rao et al. (1976) was used in this study except that the present data have been reprocessed, removing some poor measurement segments and adjusting the navigational parameters (Short and North 1990). To our knowledge, multichannel or multispectral approaches have not yet been applied to the collection of global-scale rainfall information. In any case, the improvement of understanding for the single channel case should be a good first step toward development of multichannel algorithms.

2. Microwave radiative transfer through a rain-layer

We shall consider only horizontally polarized radiances at 19.35 GHz corresponding to the ESMR-5 observations. For simplicity, we assume nonscattering, horizontally stratified hydrometeors. Wilheit et al. (1977) showed that scattering by raindrops becomes important when the rainrate exceeds 20 mm/h at 19.35 GHz, and reduces outgoing radiances at higher rain rates providing a double valued T–R relation (brightness temperature versus rainrate). Unfortunately, we have no additional information to classify heavy or light rainrates using only single frequency radiance observations. However, we base some of our optimism on the fact that in many analyses of GATE (= GARP Tropical Atlantic Experiment; GARP = Global Atmospheric Research Program) radar observations of rain rate in the Intertropical Convergence Zone (ITCZ). For example, McConnell and North (1987) and Kedem et al. (1990) showed, using GATE data, that less than about one quarter of the rain falls at rates above 20 mm/hr. Finally, the detailed comparison of ESMR-5 data with coincident GATE data suggests that the neglect of scattering does not introduce appreciable error (at least in the ITCZ case). We have therefore neglected scattering in this study, although doing so may lead to an underestimate of the actual rain rate.

In such a case, the equation of radiative transfer with the Rayleigh–Jeans approximation at microwave frequencies may be simplified to read

$$T_B(\infty) = \epsilon T_s \exp\left\{-\int_0^\infty \alpha(z')\frac{dz'}{\mu}\right\} + (1-\epsilon)\exp\left\{-\int_0^\infty \alpha(z')\frac{dz'}{\mu}\right\}\int_0^\infty \alpha(z')T(z') \times \exp\left\{-\int_0^z \alpha(z')\frac{dz'}{\mu}\right\}\frac{dz}{\mu} + \int_0^\infty \alpha(z')T(z') \times \exp\left\{-\int_z^\infty \alpha(z')\frac{dz'}{\mu}\right\}\frac{dz}{\mu}, \quad (1)$$

where $T_B(\infty)$ is the brightness temperature measured by satellite (taken here to be infinitely above the surface); ϵ the surface emissivity; T_s the surface temperature; $\mu = \cos(\theta)$, the cosine of the zenith angle; and $\alpha(z)$ the total extinction (absorption) coefficient. By restricting ourselves to near nadir pixels as discussed later we can take $\mu \approx 1$ in what follows. The important sources of extinction in the microwave region are due to molecular oxygen, water vapor, nonraining cloud liquid drops, and rain drops. The absorption cross sections were taken from Meeks and Lilley (1963) for molecular oxygen, Staelin (1966) for water vapor, and Rayleigh approximation from Gunn and East (1954) for nonraining cloud liquid drops. The extinction cross section for rain drops at wavelength λ was calculated by Mie theory from the expression given by Deirmendjian (1969). In the calculation, scattering by raindrops is treated as a loss mechanism and is not included as a source. The surface emissivity (ϵ) over ocean is calculated by the facet model given by Wilheit (1979), which used the sea surface roughness distribution by Cox and Monk (1955), and modified by the observations in the microwave frequencies (Hollinger 1971). That is, for neutral stability at 20 m height wind speed w (in m/sec) above the sea surface, the normally distributed slope variance (σ_f^2) with frequency f (in GHz) is given by

$$\sigma_f^2 = (0.3 + 0.02f)(0.003 + 0.0048w).$$

The emissivity of each facet to viewing angle was calculated by using the Fresnel formula and considering the area of each facet with respect to the viewing angle. By assuming a bivariate normal distribution of slopes in space, an effective emissivity, ϵ, in (1) could be calculated by weighting according to the frequency distribution. The dielectric constant of water was given by Paris (1971) for sea water (3.5% salinity) and pure water. The Marshall Palmer raindrop size distribution was assumed up to the freezing level, and the effects of ice or snow were ignored consistent with our nonscattering assumption. Of course, ice and snow are known to have very small absorption cross sections at 19.3 GHz (Wilheit et al. 1977).

The ESMR-5 brightness temperatures were simulated by dividing the atmospheric column into many thin layers and integration of (1) for a given atmospheric condition numerically. Fig. 1 shows the results obtained by applying essentially the same atmospheric model as used by Wilheit et al. (1977) for different freezing level heights. The sea surface temperature applied was calculated from the freezing level height by applying a linear lapse rate of −6.5°C/km. Brightness temperatures after Wilheit et al. (1977) at the 4 km freezing level without scattering are plotted by a broken line for comparison. More cases for different atmospheric models were calculated and the results were fitted by the saturating exponential $T_B = A - Be^{-CR}$

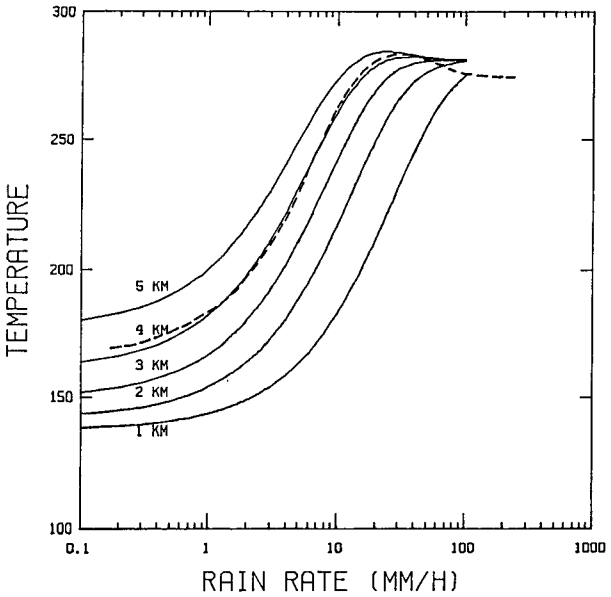

FIG. 1. Calculated brightness temperatures at 19.35 GHz (1.55 cm) as a function of rainrate for freezing levels of 1–5 km. The broken line is that of Wilheit curve without scattering.

as a T–R relation, taking A, B and C as adjustable parameters. Here A is the saturation temperature (281 K in this model) and B is the dynamic range of temperature variation. $A - B = T_0$ will be the temperature when $R = 0$, henceforth T_0 will be referred to as *background temperature.*

First, the variation of T_0 is investigated for different atmospheric conditions by changing cloud liquid water content and water vapor amounts when $R = 0$ within the scope of the Wilheit atmospheric model. Fig. 2 illustrates the variation of T_0 for different atmospheric models which include cloud water ranging from 0.0–1.0 g/m^3 of 500 m thickness below the freezing level. The relative humidity was varied from 50%–100% from surface to freezing level at 4 km height. Both effects show almost a linear relationship with brightness temperature when there is no rain. Generally, differences of 10–15 K can be realized for various atmospheric conditions given the same freezing level height over the tropical oceans. We computed the brightness temperatures in the presence of rain for the 11 different atmospheric conditions marked by circles in Fig. 2.

For a given A and T_0 (or B), the coefficient C is determined by

$$\frac{dT'}{dR} = -CT'$$

where $T' = A - T_B$. From T' and its derivative, linear regression provides the best fit for C. The results of regression fits for 11 different atmospheric conditions are summarized in Table 1 and the variation of the C with freezing level height is plotted in Fig. 3.

Table 1 shows that the coefficient of C is only a function of freezing level height. All 11 cases yield essentially the same value of C regardless of different T_0 (or B). The saturation exponential form of the T–R relation stands in very good agreement with the calculated brightness temperatures from the detailed model. In all cases the average of the magnitude of the difference between them is less than 1 K in tropical conditions (3–5 km freezing level). Figure 3 shows that the coefficient C increases with freezing level height (Z in km) possibly in a quadratic form

$$C = 0.004 + 0.026Z + 0.0045Z^2.$$

Rao et al. (1976) and Kidder and Vonder Haar (1977) used a threshold temperature for a given freezing level to identify a raining pixel. Their approaches, in other words, used fixed values of T_0 and C that were determined only by freezing level height estimated from climatology. It is easy to imagine that T_0 is different from place to place and day to day in spite of the same freezing level height as seen in Fig. 2. Rainfall retrieval from a single snapshot reduces to the problem of finding the values of T_0 and C. But in the problem of monthly averages of snapshots, the T_0 and C will fall into certain statistical distributions, possibly a normal distribution. If we find a proper way to estimate their distributions, the overall retrieval accuracy will be improved.

3. Data

The ESMR-5 calibrated brightness temperature data set from December 1973 to November 1974 was an-

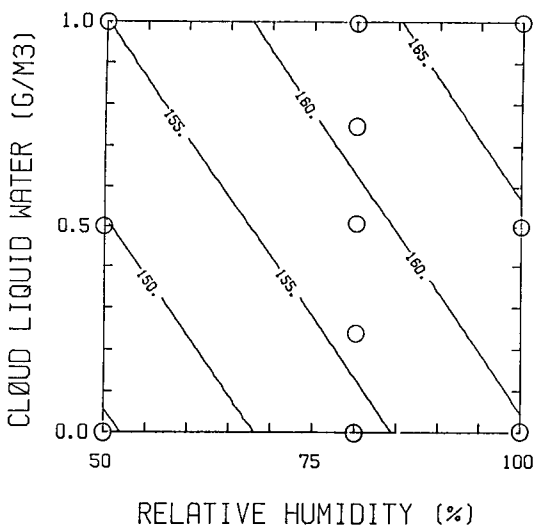

FIG. 2. Calculated background temperatures without rain at 19.35 GHz as a function of relative humidity and cloud liquid water content. The cloud is placed below freezing level with 500 m thickness. The squares indicate the atmospheric conditions that rain has been simulated.

TABLE 1. Fitted regression coefficients of T_0 and C (in parenthesis) of $T_B = A - Be^{-CR}$ for given atmospheric conditions and freezing level height. Cloud liquid water (l_c) are placed below freezing level as 500 m thick, and temperature profile is determined by a constant lapse rate of 6.5°/km from freezing level (see Wilheit et al. 1977).

		Freezing level (km) T_0 (C)				
RH (%)	l_c (g/m^3)	1	2	3	4	5
50	0.0	130 (.036)	132 (.078)	137 (.125)	144 (.179)	156 (.241)
50	0.5	136 (.036)	138 (.078)	142 (.125)	150 (.179)	161 (.241)
50	1.0	141 (.036)	143 (.077)	148 (.125)	155 (.179)	165 (.241)
80	0.0	132 (.036)	136 (.078)	144 (.125)	156 (.180)	172 (.245)
80	0.25	135 (.036)	139 (.076)	147 (.123)	158 (.177)	174 (.240)
80	0.5	137 (.036)	142 (.076)	149 (.123)	161 (.177)	177 (.240)
80	0.75	140 (.036)	144 (.076)	152 (.123)	163 (.177)	179 (.240)
80	1.0	143 (.036)	147 (.077)	154 (.125)	166 (.180)	181 (.246)
100	0.0	132 (.036)	137 (.078)	146 (.125)	160 (.181)	178 (.247)
100	0.5	138 (.036)	143 (.077)	151 (.125)	164 (.181)	182 (.247)
100	1.0	143 (.036)	148 (.077)	157 (.125)	169 (.181)	186 (.247)

alyzed. ESMR-5 measured the intensity of horizontally polarized radiation at 19.35 GHz. The instrument electronically scanned ±50 degrees across the flight path in 78 steps looking straight down. It flew in a sun-synchronous polar orbit with local noon and midnight equator crossing times [see Wilheit (1972) for more detail]. ESMR-5 had calibration problems with scan angles and different solar conditions (day and night). It also had a position error due to flexure in the antenna because of differential solar heating in day and night (Allison et al. 1974). These problems were empirically corrected by the instrument team, but the necessity of additional empirical adjustments were reported by an earlier investigator (Kidder 1976). The reprocessing efforts by Lee and Byerly (1981) improved the quality of the ESMR-5 dataset, by correcting earth location errors and identifying instrument malfunctions. Short and North (1989) found that the data still have some positioning errors (about 40 km), and empirical adjustments of both position error and scan angle bias improved the data quality drastically when they compared the ESMR-5 data with GATE radar observations.

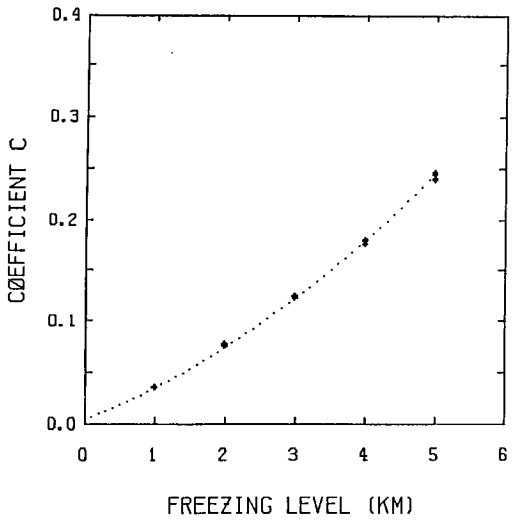

FIG. 3. The coefficient of C in the saturation exponential curve as a function of freezing level height. The dotted line is the curve fitting of $C = 0.004 + 0.026Z + 0.0045Z^2$.

In our preliminary analysis we also found that the data still contain a significant bias which is a function of scan angle. NASA initially corrected the data by using global average statistics of scan angle bias (Wilheit, personal communication). This adjustment based on a global average left significant bias on scan angles as a function of latitude, especially in the tropics. Either the same empirical adjustment concentrating in the tropics or a more adequate approach are required for correction of scan angle bias.

The original uncorrected ESMR-5 data have been extensively investigated by the authors. We have found that the scan angle bias is fairly systematic and possibly can be predicted by the radiative transfer model except for systematic differences near ±20° which are related to antenna side lobe effects (personal communication with T. Wilheit). We are currently investigating more adequate data correction methods using the microwave radiative transfer. However, at this stage we have found that the 21 pixels near nadir (scan position 29 through 49 corresponding to the swath ±12° scan angles) are fairly consistent and free of bias. But temperatures measured at night at scan positions of 36 through 43 are consistently lower by about 4 K than at adjacent positions, which suggests an instrumental problem. Therefore, an additional correction was applied to those positions at night by adding 4 K. Similar corrections were also applied by Kidder (1976) and Short and North (1989).

As a consequence the original ESMR-5 data with ±12° scan angles were used in this study. Because of the narrow scan width, a large sampling error is expected for monthly rainfall estimates. The formula proposed by Shin and North (1988) predicts about 20% sampling error on monthly 5° × 5° area averaged

rainrate estimates. Due to this data limitation, we chose to average over entire seasons in this study, and this will bring the sampling errors down to about 10%. More complete monthly based area averaged rainrate estimations should be deferred until adequate correction factors can be found and applied across the whole scan width. Due to the narrow angle observations near nadir, we can take $\mu = \cos\theta \approx 1$. Therefore, the angular dependence of microwave radiative transfer could be neglected in this study. The near nadir observing angle also eliminates the need for correcting or changing sea surface emissivity with scan angle due to the sea surface roughness (unless the wind exceeds about 7 m s^{-1} when foam breaking begins to occur). It should be noted that the horizontal resolution of ESMR-5 pixels near nadir is about 25 km.

4. Retrieval algorithm

a. Histogram analysis

At each 5° × 5° grid box, the ESMR-5 brightness temperatures for individual FOV were collected for each season over the tropical Pacific and Atlantic. The data over land and over major islands were carefully eliminated in processing. Then the collected brightness temperatures for each grid box and each season were separately partitioned into histograms with 5 K bins. Figure 4 shows an example of such a histogram. Brightness temperatures range from 130–260 K, and show a skewed distribution with a fat tail at higher temperatures. The large areas under the high temperature tail are presumed due to FOVs containing rain. The temperatures on the colder side suggest FOVs containing no rain. Although there is no rain, the background temperature, T_0, can exhibit dispersion due to different atmospheric conditions as discussed in section 2. We assume that the distribution of T_0 is normal when they are collected over a large area and for a long time. Therefore, it is assumed that the histogram is composed of the sum of normal distribution of colder temperatures of nonraining cases and rain distribution of warmer temperatures, and the peak of the histogram represents the average T_0 in that area during the season, that is, the mean of the normal distribution.

An iteration method was developed to separate the normal distribution for nonraining cases and the distribution during rain. By classifying the shape of each histogram and using the peak as a first guess of the mean of the normal distribution, the mean and variance of T_0 are estimated by searching for a best fit to the histogram. In this procedure, only the distribution of colder temperatures up to the peak + 5 K is used. Then the residual at temperatures warmer than T_0 was taken as the rain distribution. A very similar concept has recently been used in the investigation of SSM/I multichannel data by Wilheit et al. (1990).

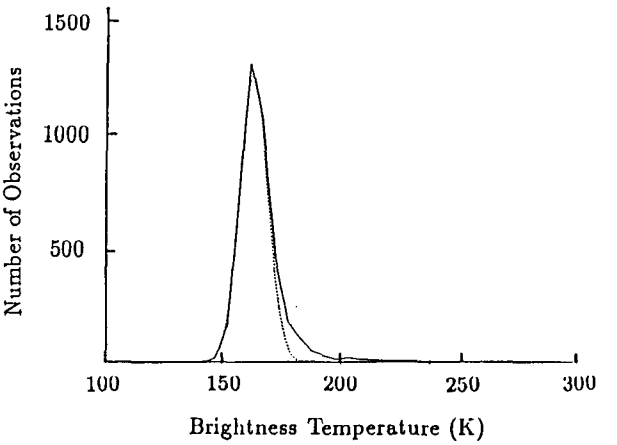

FIG. 4. An example of histogram of brightness temperatures for a season and in a 5° × 5° grid box over ocean. The dotted line indicates the best fit of normal distribution from cold temperature to the peak + 5 K of the histogram.

Figures 5 and 6 show the histograms (solid lines), fitted to normal distributions (dashed lines) at each grid box over ocean along a given latitude band. The mean and variance of the estimated normal distribution differ in each grid box. The mean gives information on the average atmospheric water vapor and cloud water, while the variance includes the fluctuation of these in space and time. The overall patterns of the mean and variance in the tropical oceans is presented in Figs. 7 and 8 and will be discussed in section 5.

b. Rain estimation

The rain probability [$P(R)$] was estimated at each grid box by considering the number of rain pixels out of the total in the histogram. The brightness temperatures of rain cases were converted to rainrates using the T–R relation discussed in section 1. Again,

$$T_B(R) = 281 - Be^{-C(z)R}$$

where $C = 0.004 + 0.026z + 0.0045z^2$, z is the freezing level height in km, and B is the dynamic range of a given background temperature. The freezing level height was estimated from zonally symmetric climatological data given by Oort and Rasmusson (1971) and Taljaard et al. (1969) as used by Kidder (1976). B is estimated from the average background temperature estimated from the peak of histogram. At each grid box, the estimated rainrate ($\hat{R}$) is

$$\hat{R} = P \sum_{i}^{N} f(T_i)\hat{R}_i(T_i)$$

where $f(T_i)$ is the probability density function of brightness temperatures when raining, and $\hat{R}_i$ is the estimated rainrate at the ith bin.

c. Beam filling error adjustment

Due to the large FOV of the microwave sensor with respect to the spatial scale of typical tropical rain, the rainfall distribution inside a FOV is hardly uniform. The sensor measures integrated radiances of nonuniform rainrates as a single value. Due to the nonlinear (saturated exponential) T–R relationship, raw rainrate retrieved from the measured radiance is not the same as the actual average rainrate. This error is called the beam filling error and has been observed in radar meteorology. Smith and Kidder (1978), Austin and Geotis (1978), and Lovejoy and Austin (1980) have addressed this problem in the case of satellite rain rate retrieval and their results showed that estimated rainrates from microwave observations consistently underestimate the observed (or simulated) rainrates by a factor of about .6 to .7, with large variances. Recently, more comprehensive studies on the beam filling problem have been conducted by Chiu et al. (1990), Short (1988), and Short and North (1990). Short's ensemble FOV model based on gamma probability distributed rainrates within a FOV predicts that the ratio of rainrate estimated from microwave sensor to actual rainrate, i.e., the beam filling correction factor, κ can be written as

$$\kappa = \frac{-F\alpha\beta}{\ln(1 + F[\{1 + \beta C\}^{-\alpha} - 1])} \qquad (2)$$

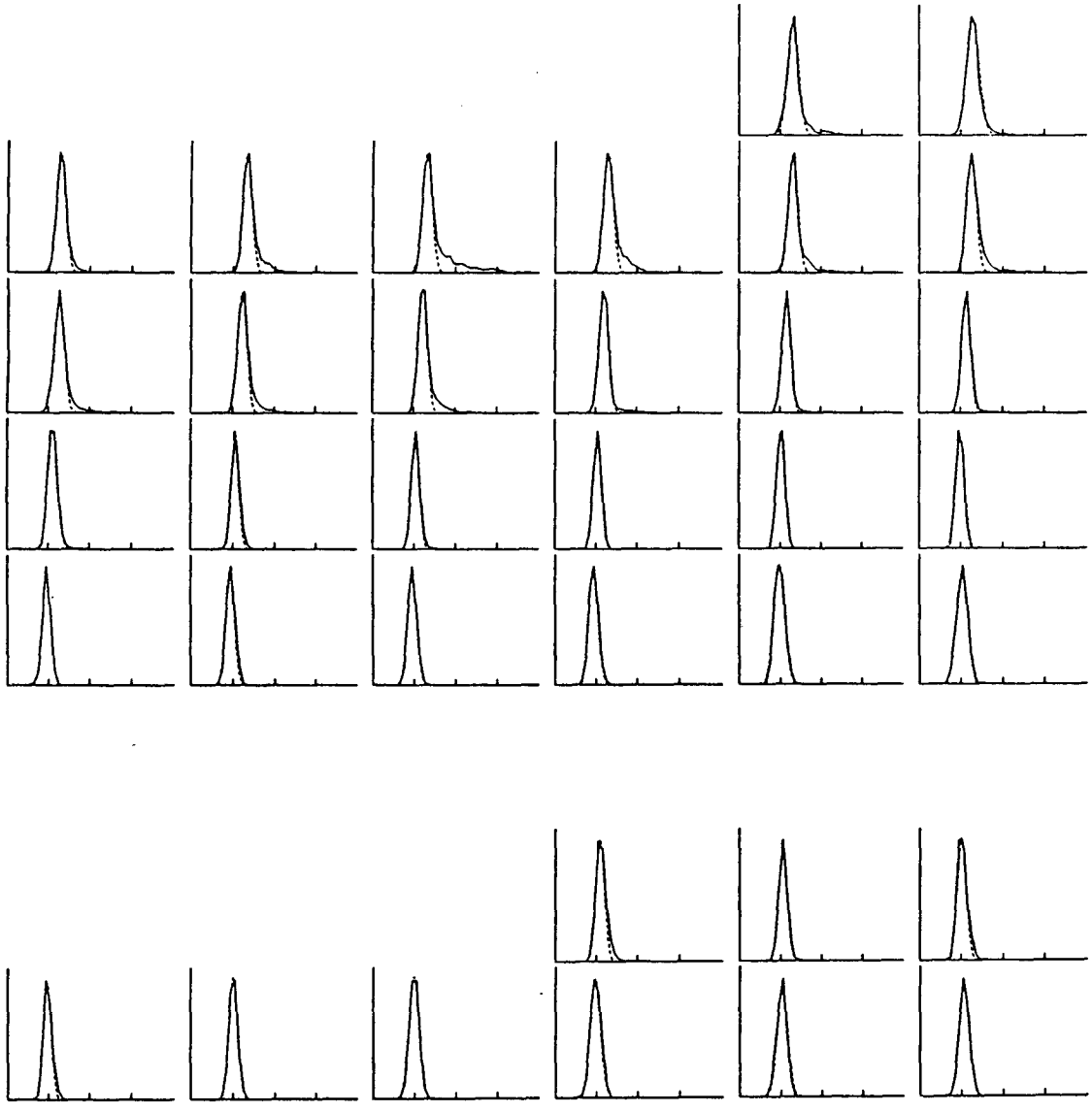

FIG. 5. Histogram (solid) and the fitted normal distribution (dashed) along a latitude band of 10°–15°S at winter. Longitude increases from left to right, top to bottom with 5°. The blanks indicate the grid areas blocked over land (see Fig. 7). The coordinates of each histogram are the same as Fig. 4. The maximum number of observations is normalized to be same.

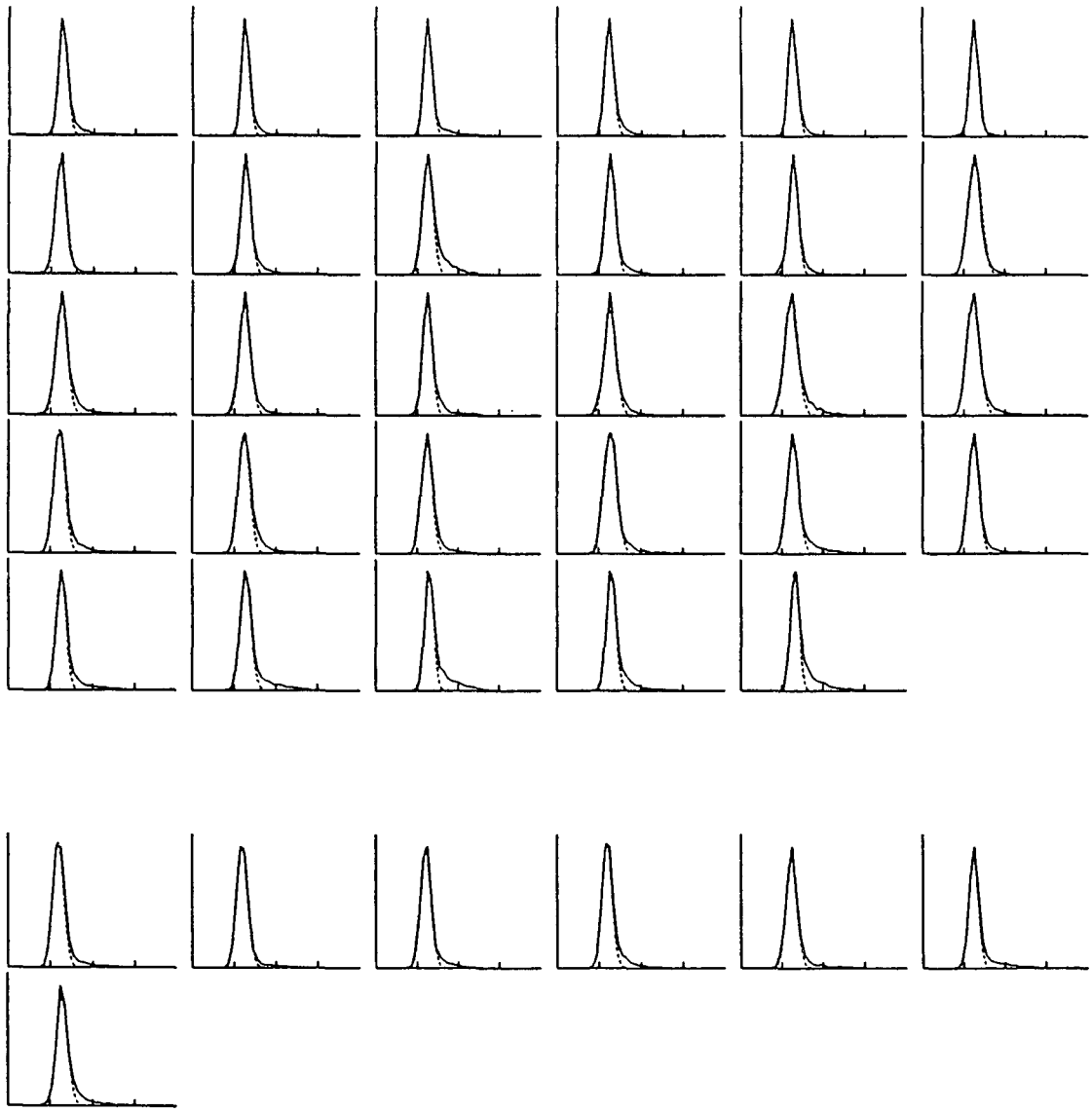

FIG. 6. Same as Fig. 5 except along a latitude band of 5°–10°N at summer.

where F is the fraction of the FOV area covered by rain, α and β are the shape and scale parameters of the gamma distribution, respectively, and C is the exponent coefficient determined by the freezing level height. Using the parameter values found in the GATE rainfall statistics from radar observations, Short estimated κ to be 2.2, and this value agrees well with the GATE rainfall from radar observations and corresponding ESMR-5 observations. These results are also consistent with the study of beam filling by Chiu et al. (1990).

It is impossible to say that whether the parameters in GATE represent Intertropical Convergence Zone (ITCZ) conditions throughout the tropics. However, in the absence of better information, the same factor of $\kappa = 2.2$ is applied to the estimated rainrate ($\hat{R}$) throughout this study. In fact, the variation of κ with time and space remains an interesting open question.

5. Results

a. Background temperature

Figure 7 shows the variation of mean background temperatures (peaks of the estimated normal distributions in histograms as in Figs. 4, 5, 6) for each season over the tropical oceans. The background brightness temperature ranges from 140 K–170 K. Figure 7 gives information about the average atmospheric water vapor and cloud liquid water contents, therefore, the high background temperature indicates that the region is generally more humid and more cloudy and vice versa.

The ITCZ and SPCZ (Southwest Pacific convergence zone) regions show generally high background temperatures, and dry regions exhibit low temperatures as expected. The movement of major convective regions and dry regions with season are well depicted. One notable fact is that background temperatures differ by about 20 K along a latitude band of the SPCZ. Therefore, the previous studies (Kidder and Vonder Haar 1977, Rao et al. 1976) that used a single threshold temperature along a latitude may be misleading in rainfall estimation or rainfall frequency.

Figure 8 shows the map of the standard deviation of the background temperatures that was estimated by a best fit to a normal distribution. This information provides the persistency of background temperatures in temporal and spatial domain in each grid box. The high values indicate that the regions undergo more fluctuation of cloudiness and water vapor in space and time and vice versa. The ITCZ and SPCZ regions show generally larger variations as compared with the dry regions, and the western parts of major oceans are generally higher than the eastern ones. Most dry regions are less than 6 K in a season, but the ITCZ and SPCZ show 6 K–10 K generally. The variation of background temperatures in winter and spring tends to be larger than during other seasons at SPCZ.

b. *Probability of rain*

Figure 9 shows the percentage of rainy pixels out of total observations in each 5° × 5° grid box for each season and annually. It shows a wide range from 4% to over 25%. The ITCZ and SPCZ regions exhibit a generally high percentage of rainy pixels, 10%–20%. In winter, the eastern Pacific at 20°–30°N shows a high percentage of raining pixels, perhaps due to the stationary fronts between the tropical and extratropical air masses. In spring and summer, these fronts are pushed to the north by the expansion of the subtropical high in the Pacific. A similar situation occurs in the southern hemisphere, yet it is less pronounced. On the other hand, in summer and fall, the southern Pacific and Atlantic extratropical latitudes have also high percentage. Some grid boxes near the coasts, especially the eastern coast of Australia and the southeastern coast of Brazil, show high rain percentages. A careful check of the histograms of these regions indicates a very long tail of high temperature in every season. It is very likely that some pixels over land are included in these histograms. ESMR-5 has been reported to have problems of antenna response due to sidelobe effects (Chesters 1979), which lead to errors near coastlines.

c. *Seasonal rainfall*

The seasonal 5° × 5° area averaged rainfall distribution of 1974 retrieved by the proposed algorithm is presented in Fig. 10. The results were compared to the precipitation climatology from ship observations for the years of 1950–72 over the Pacific by Dorman and Bourke (1979) (hereafter will be referred to as DB). However, direct comparison is not meaningful because of the difference in time and averaging area (2° latitude × 5° longitude averaging were used in DB). Larger area averaging may reduce the mean rainrate for a local scale such as with the narrow band of the ITCZ.

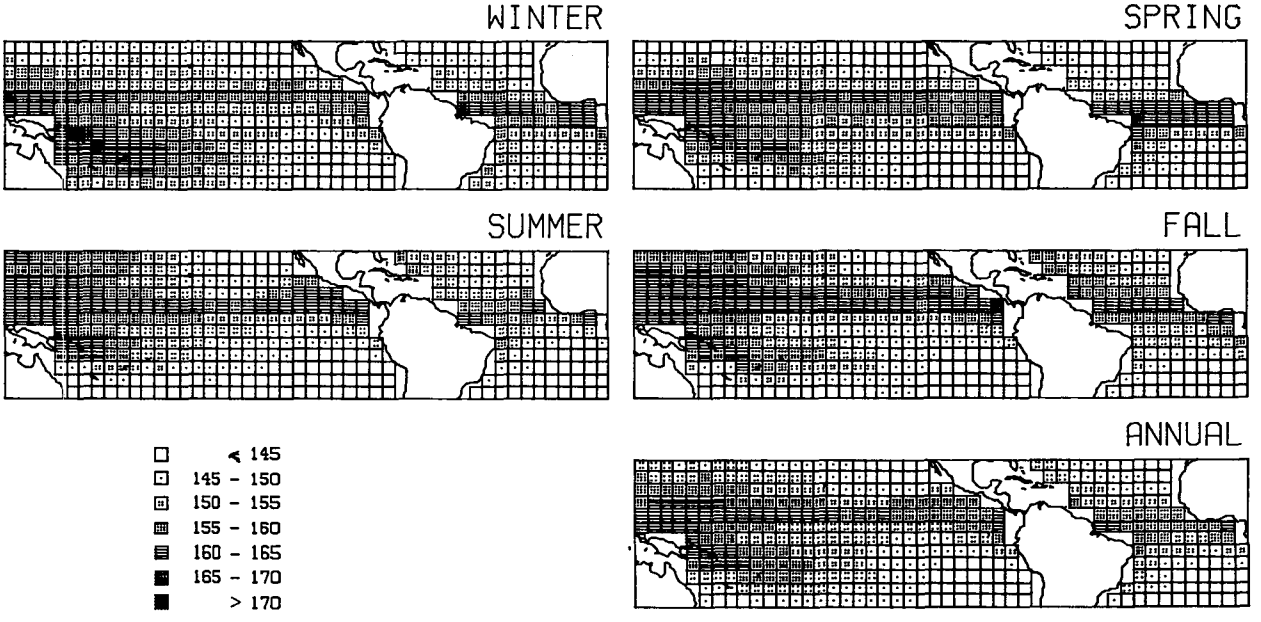

FIG. 7. Seasonal distributions of mean of background temperatures in 1974.

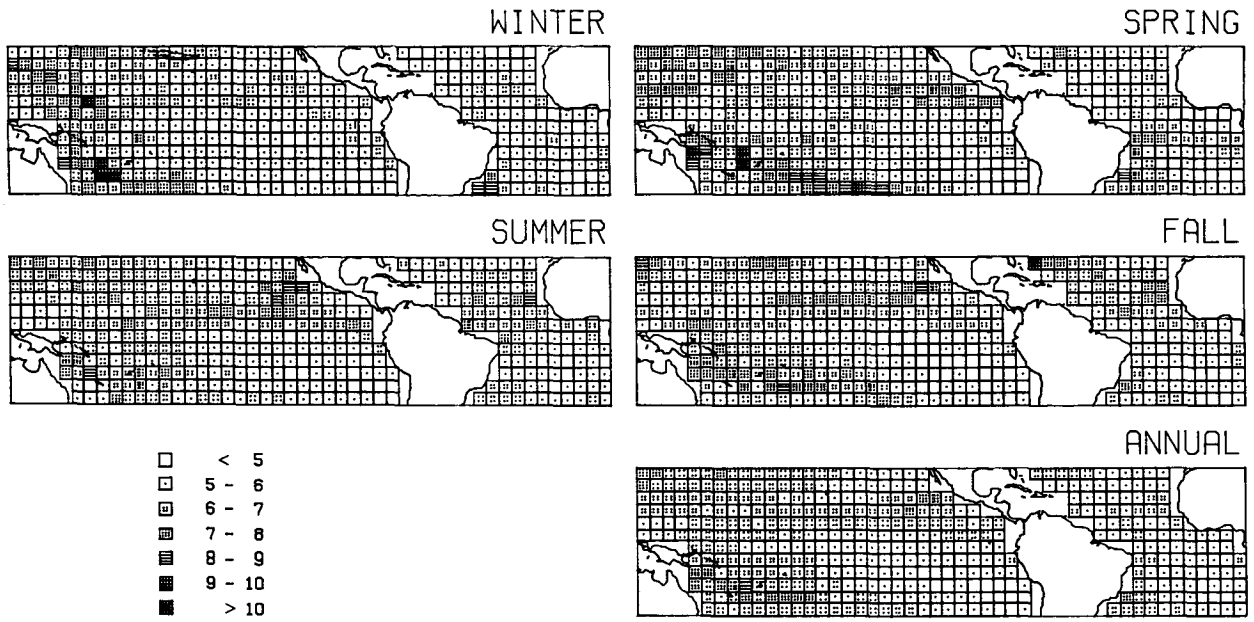

FIG. 8. Seasonal distribution of standard deviation of the background temperatures in 1974.

During December, January, and February (DJF), the ITCZ and SPCZ regions show rainfall 250–750 mm generally. But some areas in the SPCZ exhibit more than 1000 mm. The southeastern Pacific dry region shows less than 100 mm. The banded nature of ITCZ is well described. The major difference with DB in this season is at the western and central Pacific between latitudes 20° and 30°N. Our results show high rainfall exceeding 750 mm in this region while a dry region is found in DB. There are difficulties in compiling rainfall

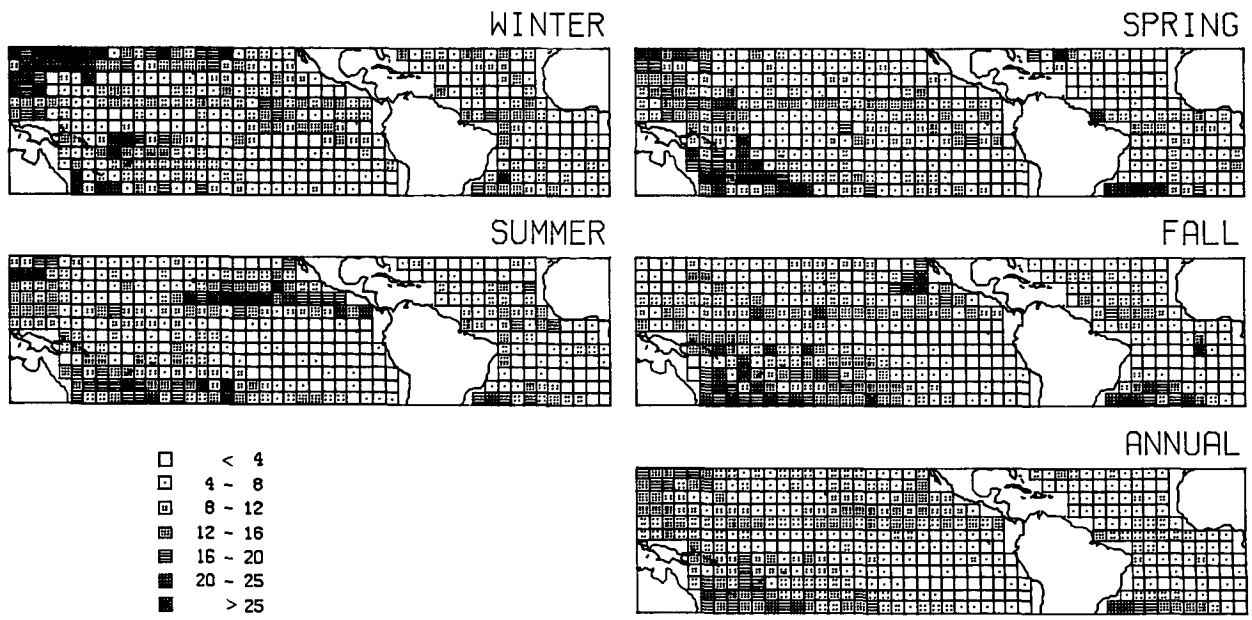

FIG. 9. Seasonal distribution of percentage of rainy pixels in 1974.

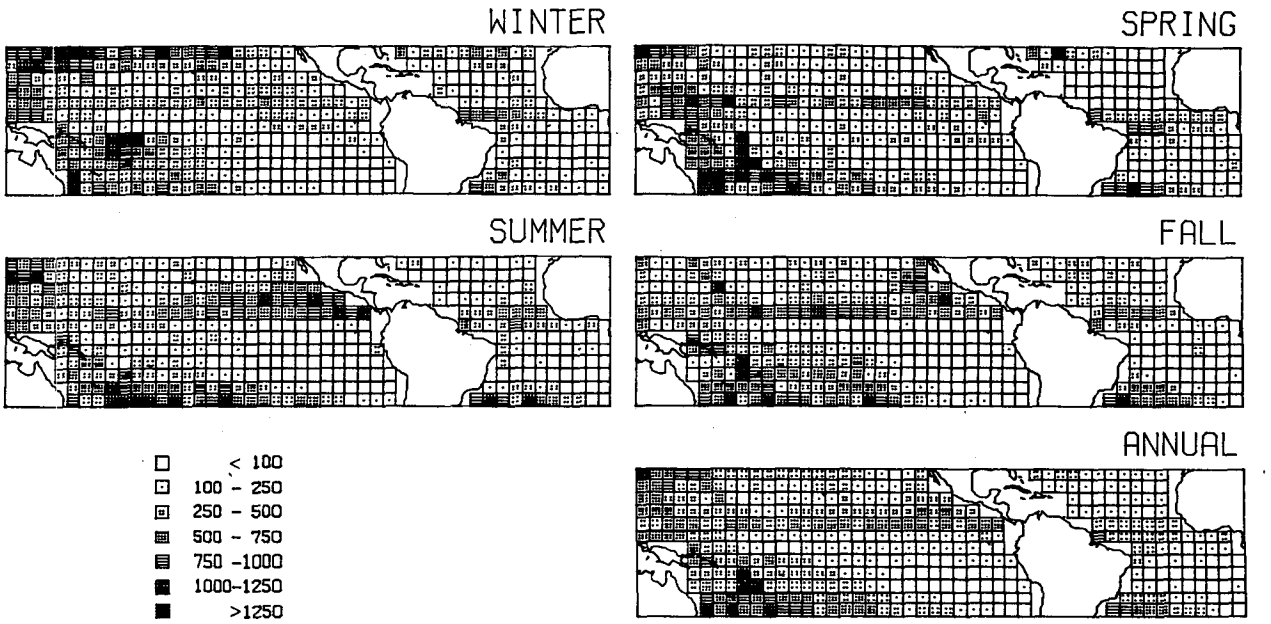

FIG. 10. The seasonal and annual rainfall (mm/season) over the Pacific and Atlantic in 1974 estimated from ESMR-5 data. The annual rainfall is multiplied by a factor of four on the given scale.

climatology over the open ocean using ship reports as DB did. Some interannual variability of rainfall is to be expected. Therefore the difference may be real but very high rainfall is suspect. According to DB, the rainy region over the northern Pacific is located between 30° and 40°N in this season. Therefore there is a chance that the midlatitude rainy region is located a little south in this year. The eastern coast of Australia also shows unexpectedly high rainfall. Except for those regions, the retrieved rainfall represents the major rainy and dry regions with comparable rainfall values with DB.

During June, July, and August (JJA), the Pacific ITCZ band intensified, especially in the central and eastern Pacific, and the Atlantic ITCZ band has been pushed north about 5°. Again, the southern latitude between 25° and 30°S in JJA shows high rainfall in both the Pacific and Atlantic. The SPCZ has weakened in this season. The movement of the major convective regions and dry regions with season is expected, and the absolute values of rainfall generally agree with DB within the uncertainty of data and analysis. However, there are several discrepancies with DB or expectation, and some of them are likely to be unrealistic.

During DJF, at 25°–30°N, rainfall seems to be overestimated. The same is true at the southern latitude in JJA. It is suggested that the rainfall at these latitudes in these seasons have extratropical characteristics which are driven by synoptic patterns rather than by convective mechanisms. Therefore the spatial scale is larger than that of tropical rainfall. Also the freezing level height is lower than in the tropics. Yet the same beam filling correction factor of 2.2 has been used as a multiplier over the entire domain. From (2), the beam filling correction factor should be different (probably smaller) because different rainfall characteristics will affect the parameters of F, α, β, and low freezing level will affect C (nonlinearity).

For all seasons, the retrieved rainfall at the east coast of Australia tends to be overestimated by the algorithm. As discussed in the section 5*b*, the histograms in this region may contain FOV over land due to the position errors. Therefore, we cannot exclude the possibility of counting the pixels over ground as a rainy pixels. Sidelobes of the antenna pattern may also enhance this effect. This effect may also be attributed to other regions containing many islands, although careful efforts to eliminate pixels over major islands have been attempted. Some high rainfall in SPCZ may be due to the contributions to the FOV by islands. However, the results suggest that the retrieved rainfall is representative of the tropical rainfall in the open ocean.

6. Conclusions

This paper has presented a new simple retrieval algorithm to estimate area-time averaged rainfall over tropical oceans by using single channel microwave measurements from satellites. The algorithm has been tested by using the ESMR-5 data and a simple microwave radiative transfer model developed in this study.

Although some problems originating with the instrument have been noted, results tend to agree with expectations based upon previous estimates of rainfall over the tropical oceans.

The saturating exponential T–R relation, $T = A - Be^{-CR}$, fits the computations based upon a nonscattering microwave radiative transfer model very well. The exponent C is determined by the freezing level, and is less sensitive to the atmospheric water vapor and cloud water amount. On the other hand, the dynamic range, B, is sensitive to both the freezing level height and atmospheric conditions. The background temperatures can differ by 20 K for different atmospheric conditions even with the same freezing level height. Therefore, we suggest that the previous studies which used a single threshold temperature to identify a raining pixel may misrepresent the rainfall frequency or rainrate over oceans.

Despite the limitations of single channel information, the retrieved rainfall agrees well in the open ocean, but has some problems near land–ocean boundaries and over islands due to the positioning errors and the sidelobe effect of the ESMR-5. If multichannel or multipolarization information is available, this problem can be effectively removed, especially by making use of the difference of horizontal and vertical polarization brightness temperatures. The series of microwave sensors developed later (the ESMR-6, SMMR, and SSM/I) can provide this information and will minimize the contamination even by small islands over oceans. It is also suggested that if the freezing level height can be estimated by multichannel information, the overall improvement will be enhanced. When TRMM flies, the active microwave sensor will provide simultaneous information on the freezing level height.

The beam filling correction factor is the most important, poorly understood parameter in the retrieval process. Our work suggests that the correction factor of 2.2 looks reasonable for most tropical convective regions, however, it is not applicable to the extratropical rainfall. More emphasis on the variation of this factor with time and space should be considered, and a practical parameterization method should be developed.

Acknowledgments. The authors wish to thank T. Wilheit and A. Chang, at NASA/GSFC for their helpful discussion and comments. We especially thank D. Short for numerous helpful suggestions and comments throughout the work. The work was supported by NASA Grants NAG 5-868 (TRMM) and NAG 5-869 (Climate and Radiation).

REFERENCES

Allison, L. J., E. B. Rodgers, T. T. Wilheit and R. Wexler, 1974: A multi-sensor analysis of Nimbus 5 data on 22 January 1973. NASA X-910-74-20, Goddard Space Flight Center, Greenbelt, MD. [NTIS Number N74-22115/1].

Austin, P. M., and S. G. Geotis, 1978: Evaluation of the quality of precipitation data from a satellite-borne radiometer. Final Report under NASA grant NSG5024, Massachusetts Institute of Technology, Cambridge, MA, 30 pp.

Chesters, D. A., 1979: A spectral filter for ESMR's sidelobe errors, NASA TM-80555, Goddard Space Flight Center, Greenbelt, MD.

Chiu, L. S., G. R. North, A. McConnell and D. A. Short, 1990: Rain estimation from satellites: Effect of finite field of view. *J. Geophys. Res.*, **95,** 2177–2186.

Cox, C., and W. Monk, 1955: Some problems in optical oceanography. *J. Marine Res.*, **4,** 63–78.

Deirmendjian, D., 1969: *Electromagnetic Scattering on Spherical Polydispersion,* American Elsevier, 290 pp.

Dorman, C. E., and R. H. Bourke, 1979: Precipitation over the Pacific Ocean, 30°S to 60°N. *Mon. Wea. Rev.*, **107,** 896–910.

Gunn, K. L. S., and T. U. R. East, 1954: The microwave properties of precipitation particles. *Quart. J. Roy. Meteor. Soc.*, **80,** 522–545.

Hollinger, J. P., 1971: Passive microwave measurements of sea surface roughness. *IEEE Trans. Geosci. Electron.*, **9,** 165–169.

Huang, R., and K.-N. Liou, 1983: Polarized microwave radiation transfer in precipitating cloudy atmospheres: applications to window frequencies. *J. Geophys. Res.*, **88,** 3885–3893.

Kedem, B., L. S. Chiu and G. R. North, 1990: Estimation of mean rain rate: Application to satellite observations. *J. Geophys. Res.*, **95,** 1965–1972.

Kidder, S. Q., 1976: Tropical oceanic precipitation frequency from Nimbus 5 microwave data, Atmospheric Science Paper 248, Colorado State University, Fort Collins, CO. [NTIS Number N76-26763/2]

——, and T. H. Vonder Harr, 1977: Seasonal oceanic precipitation frequencies from Nimbus 5 microwave data. *J. Geophys. Res.*, **82,** 2083–2086.

Kummerow, C. D., 1987: Microwave radiances from horizontally finite, vertically structured precipitating clouds, Ph.D. dissertation, Univ. of Wisconsin, Madison, WI. [NTIS Number N87-173407XSP]

Lee, D. K., and W. P. Byerly, 1981: Improvements to the Nimbus-5 ESMR calibrated brightness temperature dataset, *Final Report on NASA contract NAS5-25346,* System and Applied Sciences Corporation, Riverdale, MD.

Lovejoy, S., and G. L. Austin, 1980: The estimation of rain from satellite-borne microwave radiometers. *Quart. J. Roy. Meteor. Soc.*, **106,** 255–276.

McConnell, A. and G. R. North, 1987: Sampling errors in satellite estimates of tropical rain. *J. Geophys. Res.*, **92,** 9567–9570.

Meeks, M. L., and A. Lilly, 1963: The microwave spectrum of oxygen in the earth's atmosphere. *J. Geophys. Res.*, **68,** 1683–1703.

North, G. R., 1987: Sampling studies for satellite estimation of rain, *Preprints 10th Conf. on Probability and Statistics in Atmospheric Science, Edmonton,* Amer. Meteor. Soc., 129–135.

Oort, A. H., and E. M. Rasmusson, 1971: Atmospheric circulation statistics, NOAA Prof. Pap. 5, U.S. Dept. of Commer., Rockville, MD.

Paris, J. F., 1971: Transfer on thermal microwave in the atmosphere, Department of Meteorology, Texas A&M University, College Station, TX. [NTIS Number N72-18622].

Rao, M. S. V., W. V. Abbott and J. S. Theon, 1976: Satellite derived global oceanic rainfall atlas, NASA SP-410, Washington, D.C.

Shin, K.-S., and G. North, 1988: Sampling error study for rainfall estimate by satellite using a stochastic model. *J. Appl. Meteor.* **27,** 1218–1231.

Short, D. A., 1988: Remote sensing of oceanic rainrates by passive microwave sensors: a statistical physical approach, Ph.D. dissertation, Texas A&M University, College Station, TX.

——, and G. R. North, 1990: The beam filling error in ESMR-5 observations of GATE rainfall. *J. Geophys. Res.*, **95,** 2187–2194.

Simpson, J. R., R. Adler and G. North, 1988: A proposed tropical rainfall measuring mission (TRMM) satellite. *Bull. Amer. Meteor. Soc.*, **69,** 278–295.

Smith, E. A., and S. Q. Kidder, 1978: A multispectral satellite approach to rainfall estimates, Research report, Colorado State University, Fort Collins, CO.

——, and A. Mugnai, 1988: Radiative transfer to space through a precipitating cloud at multiple microwave frequencies. Part II: Results and analysis. *J. Appl. Meteor.*, **27,** 1074–1091.

Staelin, D. A., 1966: Measurements and interpretation of the microwave spectrum of the terrestrial atmosphere near 1 centimeter wavelength. *J. Geophys. Res.*, **71,** 2875–2881.

Taljaard, J. J., H. van Loon, H. L. Crutcher and R. L. Jenne, 1969: Climate of the upper atmosphere. Part I: southern hemisphere. vol. 1, National Center for Atmospheric Research, National Record Center and Dept. of Defense, Washington, D.C.

Wilheit, T. T., 1972: The electrically scanning microwave radiometer (ESMR) experiment, in *The Nimbus-5 User's Guide,* R. R. Sabatini, ed., pp. 59–104, NASA Goddard Space Flight Center, Greenbelt, MD.

——, 1979: A model for the microwave emissivity of the oceans' surface as a function of wind speed. *IEEE Trans. Geosci. Electron.*, **17,** 244–249.

——, A. T. C. Chang, M. S. V. Rao, E. B. Rodgers and J. S. Theon, 1977: A satellite technique for quantitatively mapping rainfall rates over the oceans. *J. Appl. Meteor.*, **16,** 551–560.

——, A. T. C. Chang and L. S. Chiu, 1990: Retrieval of monthly rainfall indices from microwave radiometric measurements using probability distribution functions. *J. Atmos. Oceanic Technol.* (submitted).

Wu, R., and J. A. Weinman, 1984: Microwave radiances from precipitating clouds containing aspherical ice, combined phase and liquid hydrometeors. *J. Geophys. Res.*, **89,** 7170–7148.